Progress In Electromagnetics Research Letters, Vol. 107, 83–91, 2022

Ultra-Wide Band Antenna on Flexible Substrate for Future Wireless Communications

Rania R. Elsharkawy[1], Khalid F. A. Hussein[2, *], and Asmaa E. Farahat[2]

Abstract—In this paper, a novel ultra-wideband (UWB) antenna with a planar single-layer structure is proposed. The antenna consists of a main circular patch that is capacitively coupled to six circular patches of very small size relative to the main patch. The coupling is achieved through narrow gaps of semicircular shape which are uniformly distributed on the circumference of the main patch. A coplanar waveguide (CPW) is used for feeding the antenna to get the complete antenna structure with the feeding line printed on one face of a flexible dielectric substrate. The antenna is fabricated and subjected to experimental assessment of its performance regarding the bandwidth, gain, and radiation efficiency. The measurements show good agreement with the simulation results. It is shown that the proposed antenna operates efficiently over the frequency band of 3.1–10.6 GHz. The antenna has a radiation efficiency that ranges from 99% to 100% over the entire band. This high efficiency is attributed to the planar single-layer structure of the antenna and the use of a thin low-loss substrate. The antenna maximum gain ranges from 2 dBi to 5 dBi over the entire frequency band. The substrate material is Rogers RO3003^{TM} which is flexible and can be conformal to planar and curved surfaces. The total substrate dimensions are $35 \times 39.4 \times 0.5$ mm.

1. INTRODUCTION

The ultra-wideband (UWB) technology has dominated nowadays in several applications. It mainly depends on the frequency band from 3.1 GHz to 10.6 GHz [1]. Operation in this band allows low power consumption and gives the ability to initiate different services in applications such as radar and safety.

UWB antennas have gained the great interest of several researchers. Different shapes and different techniques are used to obtain a UWB antenna. In [2], Saleh et al. presented a UWB antenna based on a Vivaldi tapered slot structure on a Rogers RO4003C substrate with dimensions of $42.9 \times 29.28 \times 0.813$ mm. This antenna achieves a 10.48 GHz bandwidth that ranges from 3 to 13.48 GHz with a gain ranging from 2.2 to 6.51 dBi and a radiation efficiency ranging from 90.6% to 96.7% over this frequency band. In [3], Elsharkawy et al. presented a UWB antenna based on a monopole COVID-19 virus shape with a CPW feeder. The antenna dimensions are $20.45 \times 22 \times 1.5$ mm. The antenna bandwidth ranges from 3.3 GHz to more than 60 GHz. In [4], Dwivedi et al. introduced a UWB antenna with total dimensions of $30 \times 30 \times 9.4$ mm. This antenna is based on a circular cross-slot with an artificial magnetic conductor layer to enhance the gain over the frequency band that ranges from 2.4 to 11.2 GHz with a gain ranging from 3 to 8.5 dBi. In [5], Gayatri et al. presented a UWB antenna based on a Luna shape configuration with a hexagonal ground center slot on an FR4 substrate with dimensions of $20 \times 18 \times 1.6$ mm. The frequency band of this antenna ranges from 3.09 to 11.02 GHz with radiation efficiency and gain of 99% and 5.68 dBi, respectively.

Received 19 September 2022, Accepted 14 October 2022, Scheduled 27 October 2022
* Corresponding author: Khalid Fawzy Ahmed Hussein (fkhalid@eri.sci.eg).
[1] Microstrip Circuits Department, Electronics Research Institute (ERI), Cairo, Egypt. [2] Microwave Engineering Department, Electronics Research Institute (ERI), Cairo, Egypt.

In the present work, the proposed antenna design methodology depends on a main circular patch that is printed on a single side of a thin dielectric substrate. The conducting surface on the other side of the dielectric substrate is completely removed to produce a monopole patch that acts as the main radiator of the antenna structure. Moreover, this patch is loaded with multiple parasitic circular patches of very small size relative to the main patch. For more enhancement of the bandwidth, the main patch is fed through a CPW with a wide central strip. In this way, the impedance matching bandwidth is enhanced to allow antenna operation over the UWB.

The remaining sections of the present paper are organized as follows. Section 2 explains the proposed antenna design. Section 3 is concerned with presenting and discussing both the simulated and experimental results for the performance evaluation of the proposed antenna. Section 4 gives a comparison with other related designs that are available in recent literature. The concluding remarks are given in Section 5.

2. DESIGN METHODOLOGY AND GEOMETRY OF THE PROPOSED ANTENNA

Partially closed cavities are characterized by multiple internal resonances with very narrow bands of the frequency [6]. The bandwidth of a resonant mode of an open cavity increases with increasing the aperture size with respect to the wavelength corresponding to the resonant frequency [6]. The radiation from the structures containing partially closed cavities, like the conventional microstrip patch antennas over solid ground planes, occurs through the apertures of the structure (side slots in the case of the rectangular patch). The radiation mechanism of such structures depends on the cavity resonances and occurs within very narrow frequency bands centered at the internal (or cavity) resonant frequencies. The most commonly used method to increase the bandwidth of such resonant microstrip patch antennas is to use a defected ground structure (DGS) that effectively increases the aperture size of the resonant cavity and, hence, increases the bandwidth. Also, a recently published work [7] has shown that loading the main radiator (patch) with capacitively coupled elements has the effect of enhancing the bandwidth and/or adding extra resonances to the radiating modes of the microstrip patch structures. It has been shown that using both techniques (partial removal of the ground plane and capacitive loading of the main patch with parasitic elements) [8] may result in adding more resonant frequency bands, and at the same time, improving the bandwidth of some of these radiating modes. These general rules for bandwidth enhancement of printed antenna structures are applied in the present work to suggest a design of a monopole patch antenna loaded with parasitic elements that are printed on only one side of a thin substrate. The detailed design of the proposed antenna is described in the following subsections.

2.1. Geometry of the Proposed Antenna

For UWB operation, the proposed antenna design, shown in Figure 1, depends on the complete removal of the conducting surface on one side of the dielectric substrate to produce a monopole patch antenna that is printed on the other side of the substrate. Also, four cuts are made at the center of the circular patch, which is loaded with multiple parasitic circular patches of very small size relative to the main patch. Moreover, for more enhancement of the bandwidth, the main patch is fed through a CPW with wide central strip. In this way, the impedance matching bandwidth is enhanced to get the antenna operation over the UWB. As shown in Figure 1, the proposed antenna is printed on a single face of the dielectric substrate of type Rogers RO3003$^{\text{TM}}$ of thickness $h = 0.5\,\text{mm}$, dielectric constant ε_r=3, and loss tangent $\tan\delta$=0.001. As mentioned above, the antenna consists of a main circular patch of radius R_P, with four sectorial cuts near the patch center separated with a cross-shaped strip of width W_{ST}. The main patch is loaded with six small circular patches, each of radius R_{CP}, which are capacitively coupled to the main patch through semicircular gaps, each of width G. The role of such small-size parasitic elements is to facilitate the impedance matching over the higher frequencies of the UWB through capacitive coupling to the main patch. Due to their small size relative to the main patch, these parasitic elements have almost no effect near the lower frequencies of the UWB. The complete dimensional parameters of the antenna geometry are presented in Figure 1.

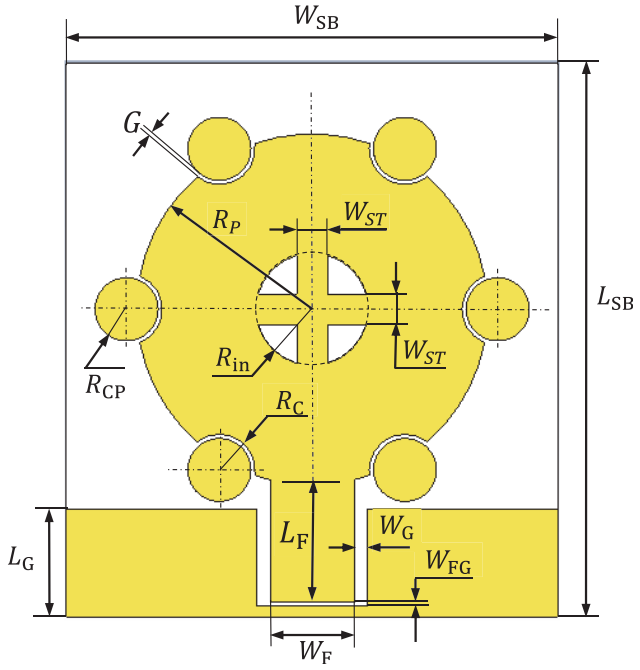

Figure 1. Design and dimensional parameters of the proposed UWB antenna.

2.2. Parametric Study for Optimum Design of the Proposed Antenna

Some general design rules of the antenna have been applied to enhance the bandwidth of the proposed antenna as described in the introductory part of Section 2. These rules include the removal of the underlying ground plane, making apertures near the patch center, capacitive loading of the antenna with multiple small elements, printing the antenna structure on a single face of the dielectric substrate, and, finally, feeding the antenna through a CPW. For further enhancement of the bandwidth to get the antenna efficiently operational over the UWB and to set the start and end frequencies exactly at 3.1 and 10.6 GHz, the dimensional parameters, presented in Figure 1, should be optimized. For this purpose, an extensive parametric study including the antenna dimensional parameters presented in Figure 1 is performed using the CST® simulator. The effects of some dimensional parameters on the impedance matching bandwidth are studied and discussed in the present subsection. The most important dimensional parameters are the radius of the main patch, R_P, the radius of the circumferential cuts, R_C, the width, G, of the semicircular gap between the main patch and each of the parasitic elements, and the length, L_G, of the CPW region.

Changing the radius of the main circular patch, R_P, has a noticeable effect on the frequency response of the reflection coefficient, $|S_{11}|$, as shown in Figure 2. Setting $R_P = 12.5$ mm satisfies the impedance matching ($|S_{11}| < -10$ dB) over the UWB (3.1–10 GHz). For values of R_P lower than or greater than 12.5 mm, the impedance matching is not satisfied over the entire band.

The effect of changing the length, L_G, of the CPW feeder on the frequency response of $|S_{11}|$ is presented in Figure 3. It is shown, from such parameter sweep, that setting $L_G = 7.7$ mm realizes $|S_{11}| < -10$ dB over the UWB. Also, it is shown that lower or greater values of L_G do not satisfy the required impedance matching over the complete UWB.

The effect of changing the radius, R_C, of the semicircular cuts (distributed over the circumference of the main patch) on the frequency response of $|S_{11}|$ is presented in Figure 4. It is shown that changing this parameter has almost no effect on the lower frequencies (2–4 GHz) of the investigated frequency range. However, it has considerable effects on $|S_{11}|$ at the higher frequencies of the operational band. This can be attributed to the fact that this parameter is responsible for controlling the capacitive load caused by coupling the small parasitic patches to the main patch. Setting $R_C = 2.55$ mm gives the most appropriate condition of the capacitive coupling to satisfy impedance matching over the entire UWB.

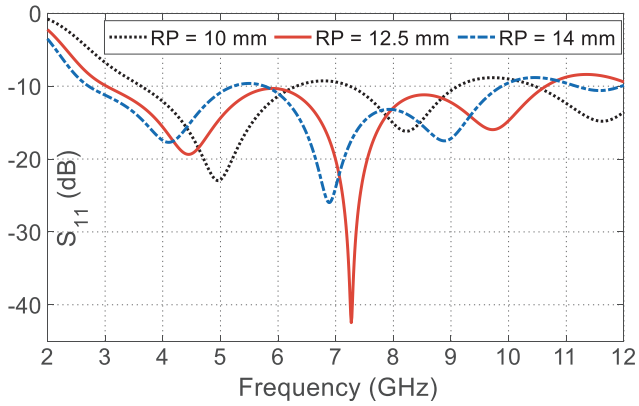

Figure 2. Frequency dependence of $|S_{11}|$ for different values of the main patch radius, R_P.

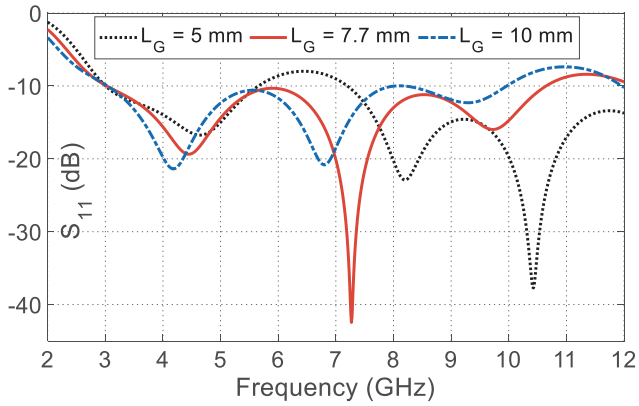

Figure 3. Frequency dependence of $|S_{11}|$ for different values of the length, L_G, of the CPW feeder.

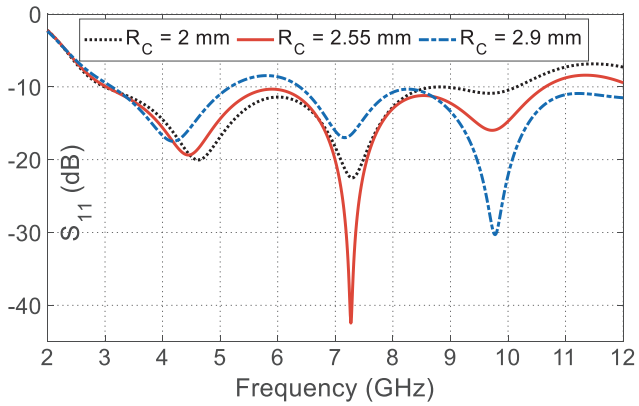

Figure 4. Frequency dependence of $|S_{11}|$ for different values of the radius R_C, of the semicircular cuts distributed over the circumference of the main patch.

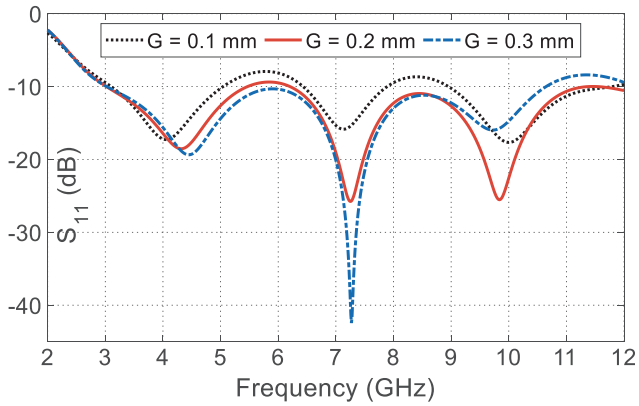

Figure 5. Frequency dependence of $|S_{11}|$ for different values of the width G of the gap between the main patch and the circular parasitic elements.

Changing the width, G, of the gap between the main patch and circular parasitic elements affects the frequency response of $|S_{11}|$ as shown in Figure 5. This parameter controls the capacitive load caused by coupling the main patch to the small parasitic patches, and hence, it does not affect $|S_{11}|$ near the lower frequencies (2–4 GHz) of the investigated frequency range. However, it has clear effects on $|S_{11}|$ over the higher frequencies. As shown in Figure 5, setting $G = 0.3$ mm satisfies the required impedance matching over the entire UWB.

2.3. Optimum Design of the Proposed Antenna

Extensive parametric study guided by those presented in Section 2.2 has been achieved through electromagnetic simulation using the commercially available CST® simulator to arrive at the optimum values of the dimensional parameters of the antenna design presented in Figure 1. The values of the dimensional parameters that realize impedance matching ($|S_{11}| < -10$ dB) over the UWB (3.1–10.6 GHz) are listed in Table 1.

Table 1. Optimum dimensional parameters for the antenna design presented in Figure 1.

Parameter	L_F	W_F	W_G	L_G	W_{FG}	R_P	R_{in}	G	R_{CP}	R_C	W_{ST}	W_{SB}	L_{SB}
Value (mm)	8.75	6	0.95	7.7	0.3	12.5	4	0.3	2.25	2.55	2.2	35	39.4

3. SIMULATION AND EXPERIMENTAL RESULTS

This section is concerned with the presentation and discussion of the simulation results and experimental measurements performed for the assessment of the proposed UWB antenna performance.

3.1. Antenna Fabrication and Measurement of Return Loss

A prototype of the proposed UWB antenna is fabricated for the verification of simulation results. As stated before, the substrate material is Rogers RO3003 with $\epsilon_r = 3$, $\tan\delta = 0.001$, and $h = 0.5\,\text{mm}$. The fabricated antenna is presented in Figure 6. The fabrication is performed using the lithography technique on only one layer of the substrate. The bottom layer of the substrate is free from any conducting elements. An SMA connector is welded to the central conductor and the side ground planes of the CPW feeder as shown in Figure 6(a). The antenna is connected to port 1 of the vector network analyzer (VNA) of Agilent FieldFox® model N9918A as shown in Figure 6(b) for measuring the reflection coefficient S_{11} at the antenna feeding port.

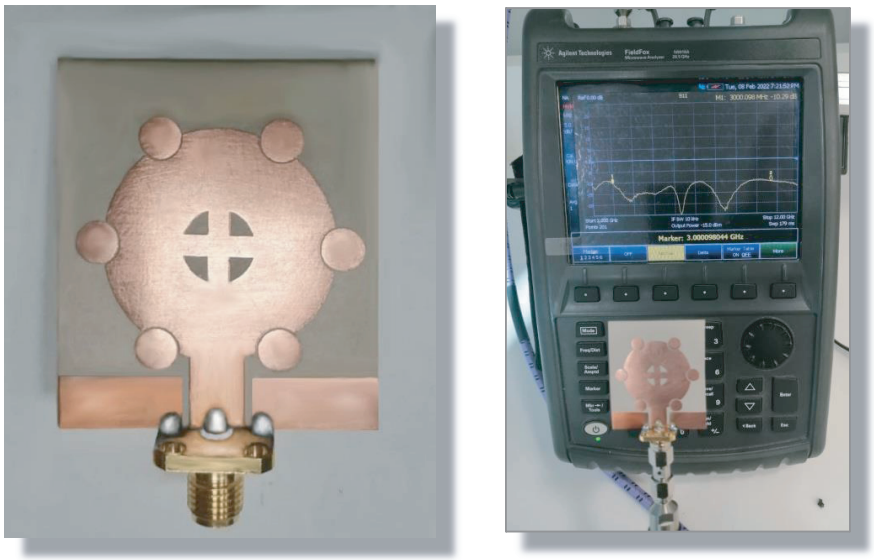

(a) (b)

Figure 6. (a) Fabricated prototype of the proposed UWB antenna. (b) Experimental setup for measurement of the reflection coefficient, S_{11} at the antenna port.

The frequency dependence of the reflection coefficient magnitude, $|S_{11}|$ and the corresponding voltage standing wave ratio (VSWR) are presented in Figure 7. The experimental measurement shows satisfactory agreement with the simulation results, and both of them show that the antenna impedance is matched over the frequency band 3.1–10.6 GHz, where $|S_{11}| < -10$ and VSWR < 2.

3.2. Gain and Radiation Patterns

The far field is evaluated using the CST® simulator as well as the experimental measurement. In this section, the radiation patterns, antenna maximum gain, and radiation efficiency are presented for

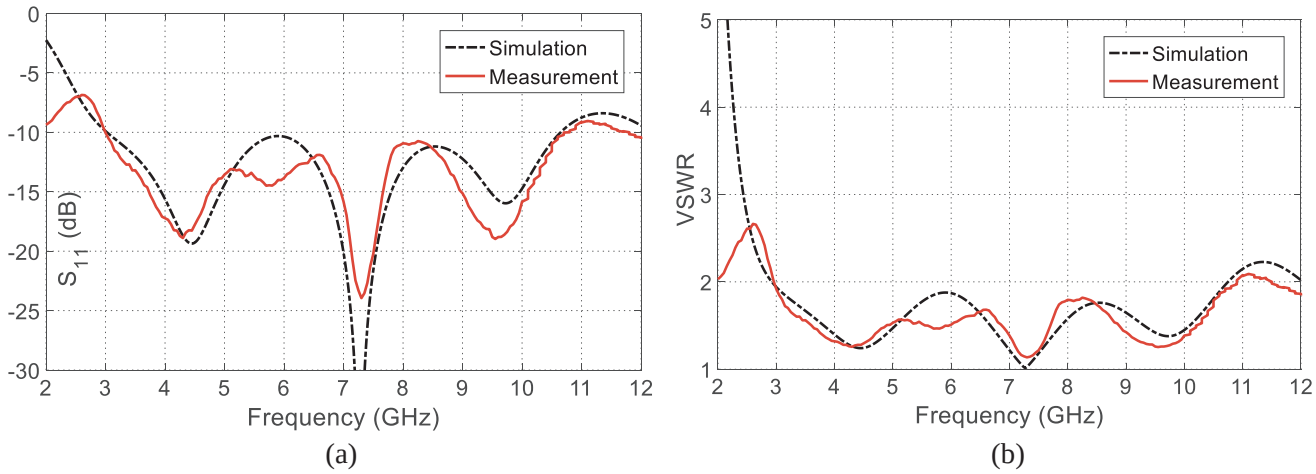

Figure 7. Frequency dependence of the (a) reflection coefficient magnitude, $|S_{11}|$ and (b) VSWR of the proposed UWB antenna.

complete assessment of the proposed antenna performance.

3.2.1. Experimental Setup for Measurement of the Gain and Radiation Patterns

The equipment presented in Figure 8 is used for measuring the gain, radiation patterns and radiation efficiency of the proposed antenna. Rhoda and Schwarz Rhode VNA model ZVA-67 is used to act as a transmitter/receiver for this purpose. A reference horn antenna model A-info LB-10180-NF (1–18 GHz) is connected to port 1 of the VNA whereas the antenna under test (AUT) is connected to port 2 of the VNA. The input power is set by commanding the VNA, and the radiated power density is measured at the different directions over the entire space ($\phi = 0 - 2\pi,\ \theta = 0 - \pi$) while the antenna rotator scans the entire space. Thus, the total radiated power can be evaluated by integration over the entire space. Hence, the radiation efficiency can be evaluated experimentally.

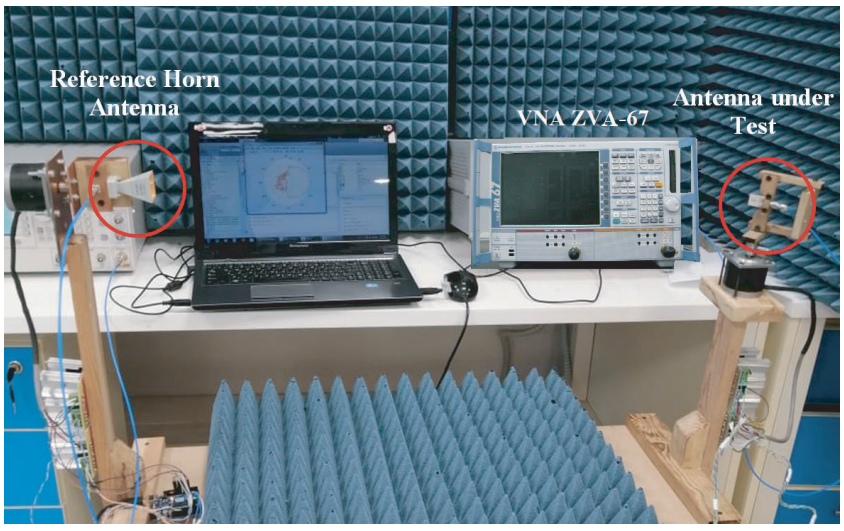

Figure 8. Experimental apparatus for measuring the gain and radiation patterns of the proposed UWB antenna.

3.2.2. Radiation Patterns of the Proposed Antenna

The radiation patterns of the total far field produced by the proposed antenna are evaluated using simulation as well as experimental measurements. The radiation patterns at 4, 6, 8, and 10 GHz in the elevation planes $\phi = 0°$ (plane of the antenna structure) and $\phi = 90°$ (plane of symmetry of the antenna) are presented in Figures 9(a), 9(b), 9(c), and 9(d). These results are obtained by electromagnetic simulation. It is shown from the radiation patterns that the antenna is almost omnidirectional over most of the operational frequency band.

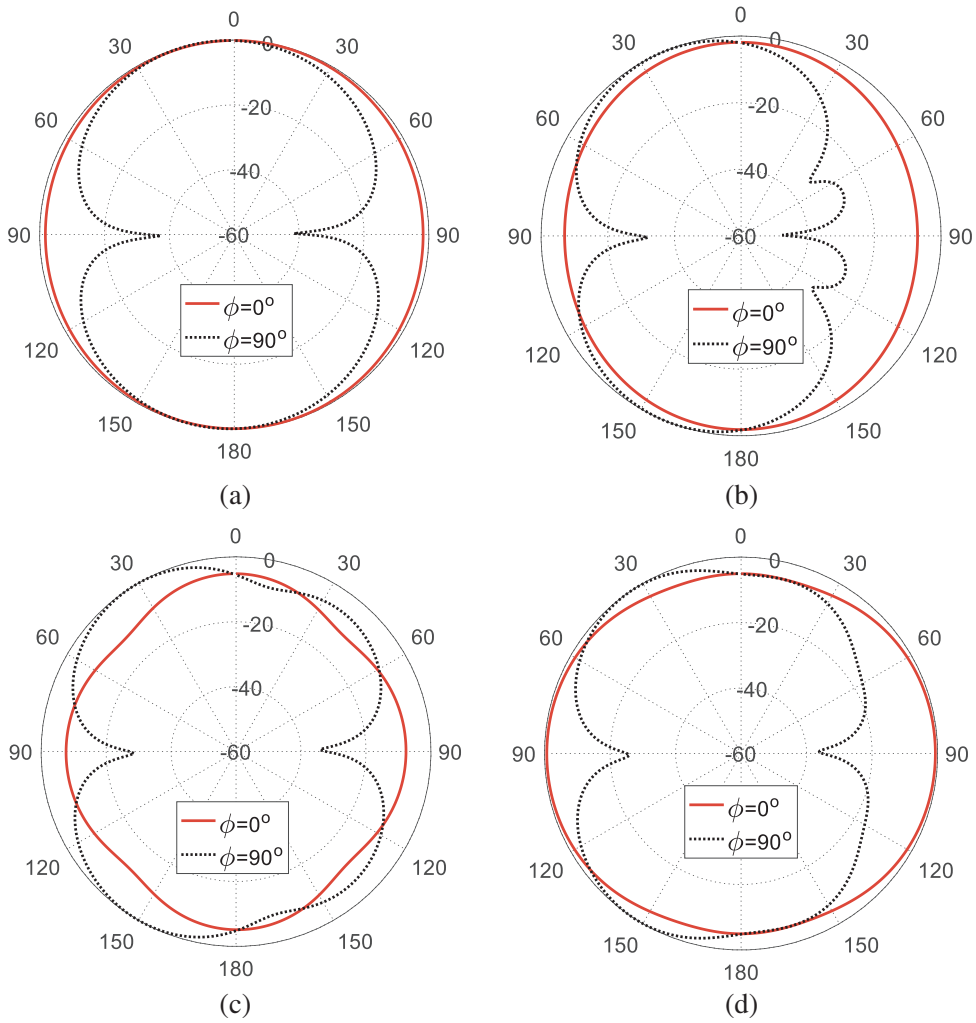

Figure 9. Radiation patterns obtained by the CST® simulator in the elevation planes $\phi = 0°$ and $\phi = 90°$ at (a) 4 GHz, (b) 6 GHz, (c) 8 GHz, and (d) 10 GHz.

The experimental method mentioned in Section 3.2.1 is used to measure the radiation pattern at 7 GHz in the elevation planes $\phi = 0°$ and $\phi = 90°$. As shown in Figure 10, the simulation and measurement show good agreement and emphasize that the antenna has almost omnidirectional patterns.

3.3. Gain and Radiation Efficiency

The assessment of the antenna performance should include the evaluation of the maximum gain and radiation efficiency over the entire frequency band. The dependence of the maximum gain on the frequency over the band (2–11 GHz) is presented in Figure 11. The experimental measurements show

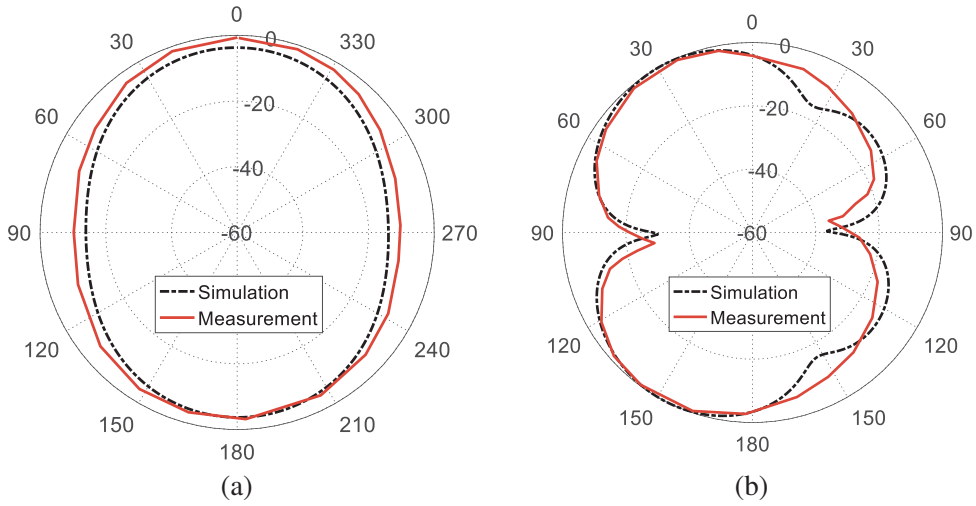

Figure 10. Radiation patterns obtained at 7 GHz by the CST® simulator as well as the experimental measurements in the elevation planes (a) $\phi = 0°$ and (b) $\phi = 90°$.

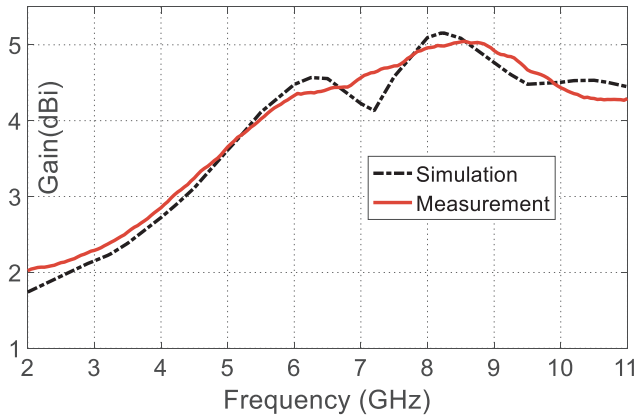

Figure 11. Frequency dependence of the maximum gain of the proposed UWB antenna.

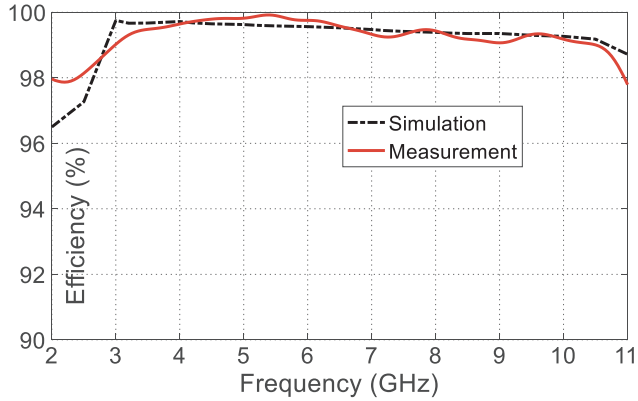

Figure 12. Frequency dependence of the radiation efficiency of the proposed UWB antenna.

good agreement with the simulation results. It is shown that the maximum gain changes with the frequency where it ranges from 2 dBi to 5 dBi over the entire frequency band and reaches its maximum value (about 5 dBi) near 8 GHz. The dependence of the radiation efficiency on the frequency is presented in Figure 12. Both the experimental measurement and simulation results show that the radiation efficiency of the proposed antenna ranges from 99% to 99.8% over the frequency band of 3.1–10.6 GHz.

4. COMPARISON WITH PUBLISHED WORK

The performance measures including the bandwidth, gain, and radiation efficiency together with the antenna dimensions achieved in the present work are compared to those of UWB antennas presented in some recently published work. A list of the compared performance measures is presented in Table 2.

Table 2. Comparison between the proposed antenna and other related works.

Work	Frequency Bandwidth (GHz)	Gain (dBi)	Radiation Efficiency %	Radiator Dimensions (mm^3)	Substrate Material
[2]	3–13.48	2.2–6.51	90.6–96.7	$42.9 \times 29.3 \times 0.81$	Rogers RO4003C
[4]	2.4–11.2	3–8.5	NA	$30 \times 30 \times 9.4$	FR-4
[5]	3.09–11.02	1.5–5.68	75–98	$20 \times 18 \times 1.6$	FR-4
[present]	3.1–10.6	2.15–5.09	99–99.8	$35 \times 39.4 \times 0.5$	Rogers RO3003

5. CONCLUSION

A novel UWB antenna has been proposed in the present work. The proposed antenna produces a wide frequency band ranging from 3.1 GHz to 10.6 GHz. The antenna design is based on employing a main circular patch surrounded by six parasitic elements that are capacitively coupled to the main patch through narrow semi-circular gaps. The antenna is fabricated and subjected to experimental assessment. Both the simulated and experimental results show that the proposed UWB antenna operates efficiently over the entire frequency band. The antenna gain ranges from 2 dBi to 5 dBi with a peak of 5 dBi near 8 GHz, and a radiation efficiency higher than 99% over the whole frequency band.

REFERENCES

1. First Report and Order, Part 15, Federal Communications Commission (FCC), Washington, DC, USA, 2002.
2. Saleh, S., W. Ismail, I. S. Z. Abidin, M. H. Jamaluddin, M. H. Bataineh, and A. S. Alzoubi, "Compact UWB Vivaldi tapered slot antenna," *Alexandria Engineering Journal*, Vol. 61, 4977–4994, 2022.
3. Elsharkawy, R. R., A. S. Abd El-Hameed, and S. M. El-Nady, "Quad-port MIMO filtenna with high isolation employing BPF with high out-of-band rejection," *IEEE Access*, Vol. 10, 3814–3824, 2022.
4. Dwivedi, R. P., M. Z. Khan, and U. K. Kommuri, "UWB circular cross slot AMC design for radiation improvement of UWB antenna," *International Journal of Electronics and Communications (AEÜ)*, Vol. 117, 1–8, 2020.
5. Gayatri, T., G. Srinivasu, D. M. K. Chaitanya, and V. K. Sharma, "A compact Luna shaped high gain UWB antenna in 3.1 GHz to 10.6 GHz using FR4 material substrate," *Materials Today: Proceedings*, Vol. 49, 359–365, 2022.
6. Hussein, K. F. A., "Effect of internal resonance on the radar cross section and shield effectiveness of open spherical enclosures," *Progress In Electromagnetics Research*, Vol. 70, 225–246, 2007.
7. Farahat, A. E., K. F. A. Hussein, and M. A. El-Hassan, "Design methodology of multiband printed antennas for future generations of mobile handsets," *IEEE Access*, Vol. 10, 75918–75931, 2022.
8. Farahat, A. E. and K. F. A. Hussein, "Dual-band (28/38 GHz) wideband MIMO antenna for 5G mobile applications," *IEEE Access*, Vol. 10, 32213–32223, 2022.